



RESEARCH ARTICLE

10.1002/2014JG002838

Key Points:

- A dynamic vegetation model simulated water cycling and vegetation productivity
- Two aridity indices were used for calculating stomatal conductance in the model
- Simulation results differ with aridity index under a warming trend over Africa

Supporting Information:

- Figure S1
- Figure S2
- Supporting Information S1

Correspondence to:

H. Sato,
hsato@jamstec.go.jp

Citation:

Sato, H., T. Kumagai, A. Takahashi, and G. G. Katul (2015), Effects of different representations of stomatal conductance response to humidity across the African continent under warmer CO₂-enriched climate conditions, *J. Geophys. Res. Biogeosci.*, 120, 979–988, doi:10.1002/2014JG002838.

Received 26 OCT 2014

Accepted 22 APR 2015

Accepted article online 5 MAY 2015

Published online 30 MAY 2015

©2015. The Authors.

This is an open access article under the terms of the Creative Commons Attribution-NonCommercial-NoDerivs License, which permits use and distribution in any medium, provided the original work is properly cited, the use is non-commercial and no modifications or adaptations are made.

Effects of different representations of stomatal conductance response to humidity across the African continent under warmer CO₂-enriched climate conditions

Hisashi Sato¹, Tomo'omi Kumagai², Atsuhiko Takahashi², and Gabriel G. Katul^{2,3}

¹Department of Environmental Geochemical Cycle Research, Japan Agency for Marine-Earth Science and Technology, Yokohama, Japan, ²Hydrospheric Atmospheric Research Center, Nagoya University, Nagoya, Japan, ³Nicholas School of the Environment, Duke University, Durham, North Carolina, USA

Abstract General circulation models (GCMs) forecast higher global vapor pressure deficit (VPD) but unchanged global relative humidity (RH) in future climates. A literature survey revealed that 50% of Earth system models and land surface models embedded within GCMs employ RH as an atmospheric aridity index when describing stomatal conductance (*g_s*), whereas the remaining 50% employ VPD. The consequences of using RH or VPD in *g_s* models for water cycling and vegetation productivity in future climates on large spatial and temporal scales remain to be explored. Process-based global dynamic vegetation model runs, changes in the hydrological cycle, and concomitant vegetation productivity for the 21st century projected climate were conducted by altering only *g_s* responses to VPD or RH and not changing any other formulations. In the simulations of the African continent under a 21st century warming trend, both stomatal functions of VPD and RH resulted in similar geographic patterns in gross primary production (GPP). However, continental total GPP was larger for the VPD response than that for the RH response. Transpiration rates were lower, resulting in a 13% increase in water-use efficiency for the VPD response compared with its RH counterpart.

1. Introduction

Plants take up CO₂ through stomata to satisfy their carbon needs but inevitably lose water during the process [Lambers *et al.*, 1998]. The ability of stomata to exert rapid control of their aperture to minimize such water loss while maintaining CO₂ uptake is one of the primary evolutionary mechanisms that has allowed terrestrial plants to survive and spread in an otherwise desiccating atmosphere. The precise signaling and concomitant regulatory mechanisms responsible for stomatal opening in response to environmental factors, however, are not fully understood [see, e.g., Buckley, 2005]. Not surprisingly, semiempirical approaches have been employed to formulate the responses of stomatal conductance (*g_s*) to environmental and physiological factors. One of the semiempirical approaches to *g_s* focuses on regulation through environmental factors (e.g., absorbed shortwave radiation, leaf temperature, humidity, and atmospheric CO₂), assuming that these environmental factors operate independently [Jarvis, 1976]. Another approach focuses on both environmental parameters and a commonly observed positive correlation between *g_s* and the photosynthetic rate [e.g., Ball *et al.*, 1987; Collatz *et al.*, 1991; Leuning, 1995].

All of the above formulations contain an atmospheric humidity index as an independent driver but differ in their assumption as to whether relative humidity (RH) or vapor pressure deficit (VPD) best reflects the effects of such a humidity index on *g_s*. Using VPD or RH as a driver of *g_s* is an issue of primary significance in climate science given that this mechanism couples the carbon and water cycles. This issue arises because a warmer climate has minor effects on RH but increases VPD exponentially at the global scale, although regional variations are expected and in some regions both RH and VPD can increase [Held and Soden, 2000].

In observations of stomatal conductance and carbon uptake for plants under a variety of atmospheric CO₂ and air temperature, models with VPD for regulating *g_s* performed better than models with RH [Nijs *et al.*, 1997; Way *et al.*, 2011]. As well, carbon-water economic theories for leaf-gas exchange, which assume transpiration is minimized for a given gain in photosynthesis, suggest that VPD^{-0.5} must be the appropriate control of *g_s* [Damour *et al.*, 2010; Katul *et al.*, 2009, 2010; Medlyn *et al.*, 2011; Prentice *et al.*,

2014] irrespective of the precise parameterization of the biochemical demand for CO₂. However, about half of the current Earth system models (ESMs) and land surface models (LSMs) employ RH in their representation of *gs* (Appendix S3 in the supporting information). The majority of them use the *gs* representation of Ball *et al.* [1987] and Collatz *et al.* [1991], where RH is employed, or the *gs* representation of Leuning [1995] where VPD is employed. For the former representation, which has a longer history than the latter, it is less strenuous to gather model parameters from existing studies. Such situation would partly explain the persistent RH formulation for *gs* in ESMs and LSMs.

The significance of these differences in the humidity index responses of *gs* to RH or VPD in ecosystem-scale carbon and water cycling studies is rarely disputed and has been recognized for quite some time [Kumagai *et al.*, 2004]. What may be disputed is the significance of these differences in *gs* responses to RH or VPD at much larger spatial (e.g., continental) and temporal (i.e., scales pertinent to vegetation biomass dynamics) scales. It is precisely this issue that motivates this study. Specifically, changes in water cycling and vegetation productivity arising from these two representations of *gs* (i.e., as functions of RH or VPD) are explored for the future climate scenario projected for the African continent. The African continent was deemed as an appropriate case study because the geographic distribution of vegetation biomass is primarily controlled by aridity, and aridity is projected to significantly change in space and time across that continent by the end of the 21st century.

2. Methods

2.1. The Model

All model runs were conducted with the spatially explicit individual-based dynamic global vegetation model (SEIB-DGVM) [Sato *et al.*, 2007]. The modifications described by Sato and Ise [2012] were used, including new empirical rules of allometry, allocation, water stress function, and phenology developed for plant-functional types (PFTs) of African woody species, and a revised wildfire submodel “trained” and “validated” for the African continent. Following these modifications, Sato and Ise [2012] demonstrated that the model reproduced geographical distributions of the continent’s biomes, annual gross primary productivity (GPP), and biomass under current climatic conditions. The modified model is available online (<http://seib-dgvm.com/>).

A rectangular area bound by 40–S55°N and 20–E55°W was used to enclose the African continent (Figure 1). This domain was divided into 0.5 × 0.5 grid cells, and each grid cell was represented by a 30 × 30 m spatially explicit virtual forest, in which individual trees establish, compete, and die. Three PFTs exist in the modified model: tropical evergreen woody, tropical rain-green woody, and C₄ grass species. Establishment of these PFTs assume infinite seed dispersal; all PFTs had the capacity to establish under a given climatic condition and had the same chance to establish, regardless of whether they already existed in a grid cell. A previous study suggested that such an assumption promotes a more “adaptive” vegetation distribution that results in higher vegetation productivity under changing environmental conditions, as discussed elsewhere [Sato and Ise, 2012]. Hence, the changes in biomass are expected to serve as “upper limit” envelopes on productivity changes.

The SEIB-DGVM employs a semiempirical model [Leuning, 1995] for computing single-leaf stomatal conductance or *gs* (mol H₂O m⁻² s⁻¹), given as

$$gs = GS_{b1} + \frac{GS_{b2} p}{c_a - \Gamma} \frac{1}{1 + (VPD/GS_{b3})}, \quad (1)$$

where *p* is the leaf photosynthesis (μmol CO₂ m⁻² s⁻¹), VPD is the vapor pressure deficit (hPa), and *c_a* is the atmospheric CO₂ concentration (ppmv). *GS_{b1}* and *GS_{b3}* are the constants across all PFTs, set here at 0.01 (mol H₂O m⁻² s⁻¹) and 50.0 (hPa), respectively. *GS_{b2}* is a dimensionless constant. Finally, *Γ* is the CO₂ compensation point (ppmv), which increases with air temperature (*ta* in celsius) for C₃ PFTs [Brooks and Farquhar, 1985].

$$\Gamma = 35 \times \left[1.0 + 0.0451 \times (ta - 20.0) + 0.000347 (ta - 20)^2 \right] \quad (\text{for } C_3 \text{ PFTs}). \quad (2)$$

$$\Gamma = 5 \quad (\text{for } C_4 \text{ PFT}). \quad (3)$$

Note that this method of adjusting the CO₂ compensation point reduces the CO₂ fertilization effect for C₃ PFTs under a warming climate.

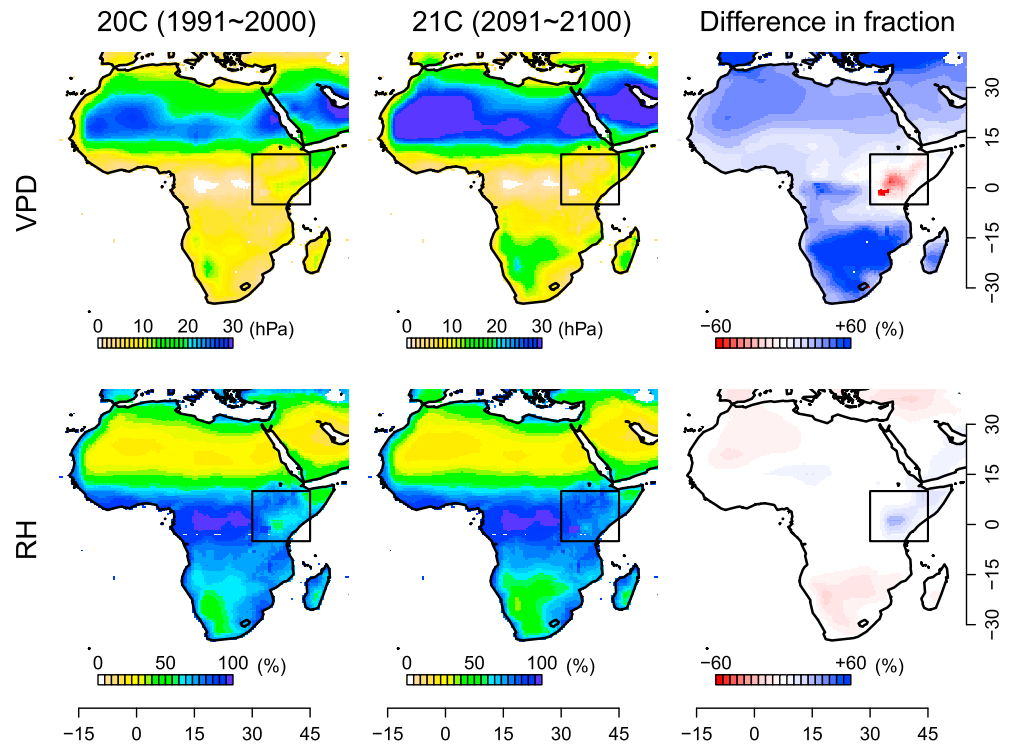


Figure 1. Comparisons of average (top) vapor pressure deficit and (bottom) relative humidity (RH) of the forcing data for current and projected climates. Daily data are averages for the last 10 years of the (left) 20th and (middle) 21st centuries. (right) Fractional changes during the 21st century. The vertical axes indicate latitude, and the horizontal axes on the left and middle columns indicate longitude. Values for the 20th century are observation-based data, whereas data on changes during the 21st century were taken from the output of an atmospheric general circulation model, which was simulated using the A1B IPCC CO₂ emission scenario. VPD generally increased throughout the continent, but changes in RH were negligible (consistent with prior expectations for the global climate system). We conducted separate analysis for the areas within squared boxes in Figure 1, where deviated pattern appeared (see main text for detail).

To address the study objectives, equation (1) was replaced by the other widely used formulation in ESMs and LSMs given by *Ball et al.* [1987] and *Collatz et al.* [1991] as

$$gs = GS_{b1} + \frac{GS_{b4} p}{c_a - \Gamma} RH, \quad (4)$$

where RH is the relative humidity (fraction) and GS_{b4} is a dimensionless constant with typical values in LSMs of 9.0 for C₃ PFTs and 4.0 for the C₄ PFT [*Collatz et al.*, 1992, 1991; *Sellers et al.*, 1996]. This formulation was modified here by including Γ , so that any difference in model results arising from the use of equations (1) and (4) can only be attributed to the difference in the representation of humidity (i.e., VPD versus RH).

We also conducted simulations without considering the effect of Γ for evaluating how the original form of the widely used stomatal conductance model changes the prediction:

$$gs = GS_{b1} + \frac{GS_{b4} p}{c_a} RH. \quad (5)$$

Hereafter, equations (1), (4), and (5) in the SEIB-DGVM will be referred to as the “VPD formulation,” “RH modified formulation,” and “RH original formulation” respectively. We employed the common set of values for the parameters GS_{b2} and GS_{b4} (i.e., 9.0 for C₃ plants and 4.0 for C₄ plants). With these parameter values, and with change of a calibration parameter LA_{max} (maximum leaf area per canopy surface of woody PFTs in m² m⁻²) from 4.0 to 3.0, all formulations roughly agree on the continental-scale GPP over the last 10 year period of the 20th century (i.e., 1991–2000); by repeating a 1100 year simulation period composed of 1000 years for spin-up and 100 years for the 20th century (see Simulation procedure section for details), the VPD, the RH modified, and the RH original formulations yielded 0.691, 0.683, and 0.690 (kg C m⁻² yr⁻¹),

respectively, for GPP when averaged over the entire simulation area during the last 10 year period of the simulation. These values are comparable to an estimate for current GPP over the simulation area ($0.713 \text{ kg C m}^{-2} \text{ yr}^{-1}$), which is based on observations and bottom-up upscaling reported by *Beer et al.* [2010].

Conventional equations describing Fickian diffusion of CO_2 from the atmosphere into leaves (reflecting atmospheric CO_2 supply; see equations (9) and (10) in the discussion for detail) and the classic photosynthetic model (reflecting atmospheric CO_2 demand) were used to compute p in equations (1), (4), and (5). The classic photosynthetic model is a Michaelis-type function of the intensity of photosynthetically active radiation [*Ito and Oikawa, 2002*], linking p to intercellular CO_2 ($= c_i$) for light-saturated photosynthesis (reflecting CO_2 demand). Hence, this system of three equations can be recursively solved for the three unknowns, g_s , p , and c_i . This computational method is further described elsewhere [*Sato et al., 2007*]. The addition of water-stress functions is also explained elsewhere [*Sato and Ise, 2012*].

2.2. Climate Data

The models for the 20th century runs were driven by measured annual means of global atmospheric CO_2 concentrations and the Climate Research Unit (CRU) observation-based climatic data [*Mitchell and Jones, 2005*]. The models for the 21st century runs were driven by the A1B scenario of rising CO_2 taken from the Intergovernmental Panel on Climate Change (IPCC) Special Report on Emission Scenarios and the Model for Interdisciplinary Research on Climate (MIROC) 3.2(medres) atmospheric general circulation model output [*Emori et al., 2005; K-1-Model-Developers, 2004*].

All of the 21st century runs were conducted after completing the 20th century runs, which served as the initial states for each of the three g_s model variants. The following steps were taken to provide consistency between data sets across centuries; the average MIROC output for 1991 to 2000 were subtracted from the MIROC 21st century projections for each climatic variable in each month and in each grid cell, and the 1991–2000 averages of the CRU were added. Both the CRU and MIROC data were provided on a monthly basis, and diurnal variability within each month was supplemented using the National Center for Environmental Prediction/National Center for Atmospheric Research (NCEP-NCAR) daily climate data [*Kalnay et al., 1996*]. Appendix A8 in *Sato and Ise* [2012] presents the detailed procedure for processing these data sets.

Figure 1 compares distributions of mean VPD and RH averaged over the last 10 years of the 20th and 21st centuries. VPD generally increased throughout the continent, but changes in RH were negligible (consistent with prior expectations for the global climate system). An exception to this general continental trend was found for the eastern part (areas within squared boxes in Figure 1), where both VPD and RH indicate a moistening trend. Appendix S1 in the supporting information shows the distribution of mean air temperature and precipitation averaged over the last 10 years of the 20th century and its changes until the last 10 years of the 21st century. Mean annual air temperature during the 21st century increased throughout the study area, with drier subtropical regions warming more than their moist tropical counterparts. Annual precipitation increased in the eastern part of the continent and the sub-Saharan but decreased in western, southern, and northern parts. The increasing trend of precipitation in the eastern part of the continent corresponds to the wetting trend of the air.

2.3. Simulation Protocols

A 1000 year spin-up run starting from bare ground was conducted for each g_s model variant by repeatedly inputting climate data for 1901–1930 and inputting 306 ppm atmospheric CO_2 , which is the global 1900 year mean. A 1000 year spin-up was deemed sufficient for the slow carbon pools (e.g., woody biomass) to reach equilibrium. Simulations for 1901–2100 were conducted for each g_s model variant after the spin-up period.

SEIB-DGVM requires hundreds of years until the vegetation structure attains equilibrium under new climatic conditions. This slow convergence to equilibrium is not surprising because a series of processes related to plant population dynamics, such as competition against existing plants, must be allowed to progress. An additional 1000 year period was appended to the end of the 21st century to obtain the equilibrium state

of the vegetation in relation to the environment at the end of the 21st century as a way to survey the effects of the possible time lag. Climate data for 2091–2100 were inputted repeatedly for these additional years, and the CO₂ concentration was held constant at expected levels for the year 2100.

Intuitive analysis of the aforementioned mentioned simulation (referred by control run hereafter) was hindered by several factors, including (1) wildfires, whose frequency and intensity may change with climatic conditions; (2) concurrent changes in climatic conditions and atmospheric CO₂; and (3) dynamic vegetation features, which change vegetation composition with climatic conditions. Hence, “no-fire,” “no-fire/fixed-CO₂,” and “no-fire/no-tree” experiments were conducted to provide a baseline reference. Wildfires in the no-fire experiment were suppressed artificially. Wildfires in the no-fire/fixed-CO₂ experiment were suppressed artificially, and further changes in CO₂ were suppressed from 2001 onward. Wildfires in the no-fire/no-tree experiment were suppressed artificially, and only the C₄ grass PFT was allowed to establish. These reference experiments were conducted for each of the three *gs* formulations with the climatic and atmospheric CO₂ data for the 20th and 21st centuries.

3. Results

Using the aforementioned climate projections for the 21st century, the GPP of the control run generally increased over a wide range of vegetated areas (Figure 2). The most conspicuous increases in GPP occurred in the eastern part of the African continent (areas within square boxes in the Figure 2), where precipitation increased significantly (Appendix S1 in the supporting information). In contrast, a slight decrease in the GPP occurred around the marginal regions of vegetation zones. The variant models exhibited nearly identical geographic patterns in the GPP changes (Figure 2). The no-fire experiment also showed a nearly identical geographic pattern in the GPP changes, whereas the no-fire/fixed-CO₂ experiment indicated nearly identical but evenly reduced geographic distribution in the GPP changes (Appendix S2 in the supporting information).

Although consistent changes were noted for the continental-scale averaged GPP trajectory during the 21st century (Figure 3), the VPD formulation showed upward changes compared to the RH formulations. In the control run, averaged GPP for the VPD, RH modified, and RH original formulations increased by 15.6, 15.0, and 14.7 (%), respectively (Table 1). The no-fire experiment revealed nearly identical GPP trajectory, while it was always higher by about 0.05 (kg C m⁻² yr⁻¹) compared to the control run. Although the no-fire/fixed-CO₂ experiment indicated a decreasing trend, the VPD formulation showed a less decrease than the RH formulations; the continental-averaged GPP for the VPD, RH modified, and RH original formulations changed by -5.4, -6.5, and -6.3 (%), respectively (Appendix S5 in the supporting information). Note that continental-scale average GPPs attained a quasi-equilibrium state with their climatic conditions for all *gs* model formulations (Figure 3).

Although the VPD formulation showed upward changes in the averaged GPP, relative to its RH counterparts, the opposite trend was found for transpiration rates. In the control run, the continental-scale transpiration rates during the 21st century changed by -4.7, -2.4, and -1.9 (%), respectively, for the VPD, RH modified, and RH original formulations (Table 1). As a result of this opposite change, the water-use efficiency (WUE) of carbon uptake became higher for the VPD formulation than for the RH formulations by the end of the 21st century (26.9, 22.0, and 21.2%, respectively, for the VPD, RH modified, and RH original formulations). The no-fire experiment indicated the same pattern of changes in the transpiration rate and WUE (Appendix S4 in the supporting information). The no-fire/fixed-CO₂ experiment showed a concurrent trend of changes in terms of a higher GPP, lower transpiration, and higher WUE for the VPD formulation than for the RH formulations (Appendix S5 in the supporting information).

The variant models in the no-fire/no-tree simulations showed opposite patterns of change for the end of the 21st century. All variant models displayed decreasing trends in the GPP throughout the continent except for the eastern part (Appendix S2 in the supporting information), where the largest precipitation increase during the 21st century was simulated (Appendix S1 in the supporting information). The magnitude of the decrease was about 3 times larger for the VPD formulation compared to that for the RH formulation: the continental-scale GPP changed by -8.9, -3.1, and -2.8 (%) until 2091–2100 for the VPD, RH modified, and RH original formulations, respectively (Appendix S6 in the supporting information). A

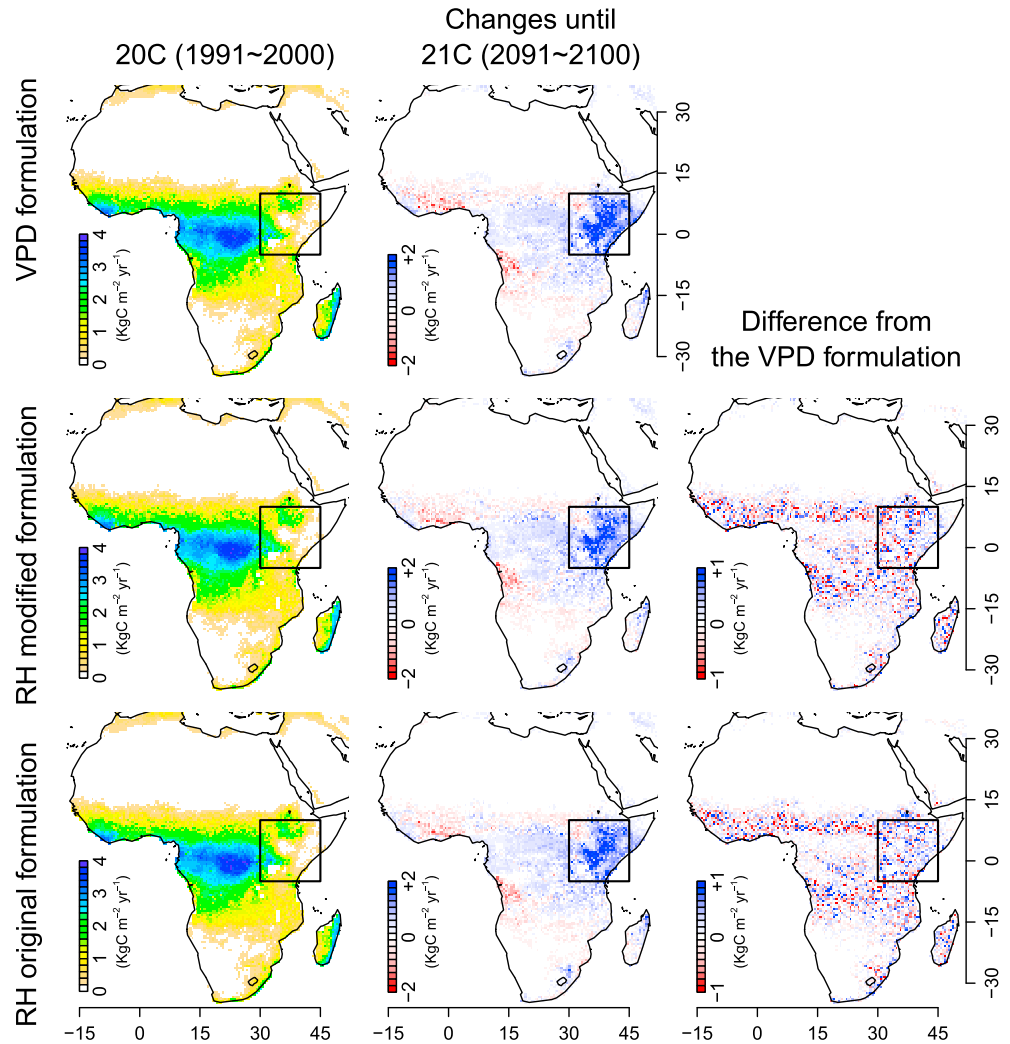


Figure 2. Comparison of the modeled gross primary production (GPP) for the three stomatal conductance model variants. Daily output were averaged over the last 10 years of the (left) 20th century, and its changes during the (middle) 21st century are presented. (right) Difference in the GPP changes during the 21st century between the model variants (changes of TH variant models were subtracted by the change of the VPD variant model). Distribution maps in the top, middle, and bottom plots were obtained with different stomatal conductance formulations. All variant models showed nearly identical geographic patterns in the GPP changes. Geographical locations of square boxes correspond to these in Figure 1.

decreasing trend was also found for the transpiration rates, in which the continental-scale transpiration changed by -7.5 , -4.4 , and -5.4 (%) until 2091–2100 for the VPD, RH modified, and RH original formulations, respectively (Appendix S6 in the supporting information). WUE increased in all conductance formulations (by 9.5, 10.3, and 11.9%, respectively, for the VPD, RH modified, and RH original formulations), but the extent of the increase was much lower than that for the control run (Table 1; 26.9, 22.0, and 21.2%, respectively, for the VPD, RH modified, and RH original formulations) and the no-fire experiment (Appendix S4 in the supporting information; 28.6, 22.5, and 21.9%, respectively, for the VPD, RH modified, and RH original formulations).

The eastern part of the African continent (areas within squared boxes in Figure 1) shows moistening trend of near-surface air during the 21st century in both VPD and RH (Figure 1) in contrast to the drying trend over the entire continent. Irrespective of such intercontinent climate differences, concurrent differences between the stomata formulations were significant: higher GPP and WUE were computed under the changing climate of the 21st century for the VPD formulation when compared to the RH formulations (Table 2).

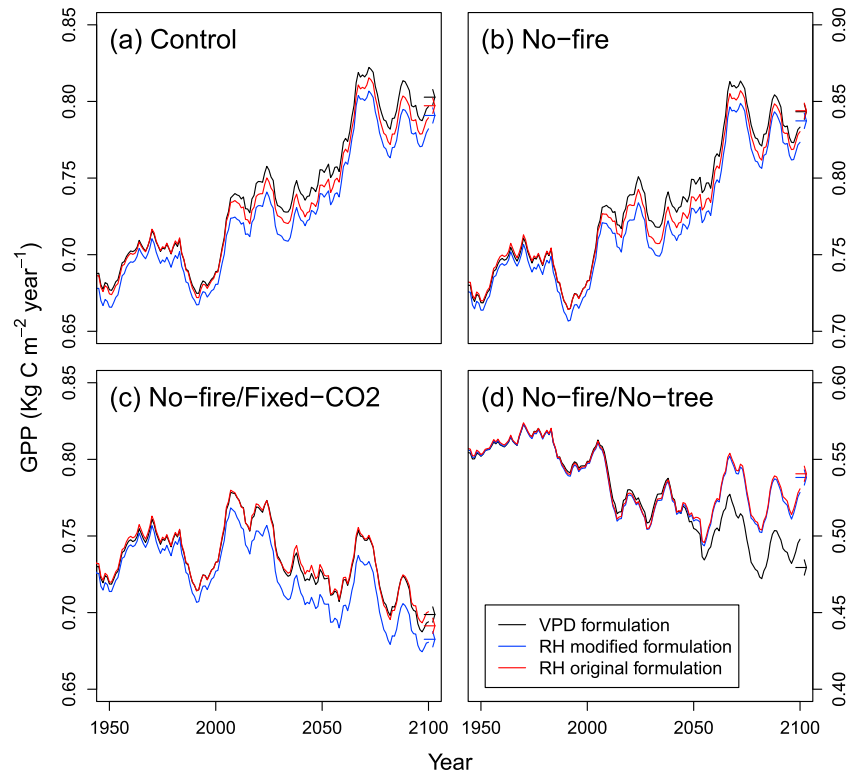


Figure 3. Trajectory lines showing the 10 year running means of the modeled annual gross primary production (GPP) during 1950–2100. The arrows on the right indicate mean values for the last 10 years of an additional 1000 year simulation with no further changes in climate and CO₂ level from 2100 onward. (a) Results of the control run. (b) Results of the no-fire experiment in which wildfires were suppressed. (c) Results of the no-fire/fixed-CO₂ experiment in which wildfires were suppressed and further changes in CO₂ were suppressed from 2001 onward. (d) Results of the no-fire/no-tree experiment in which only the C₄ grass plant functional type was established and wildfires were suppressed.

4. Discussion

The CO₂ fertilization effect was most responsible for the increasing trend in the GPP observed during the 21st century in the control run and the no-fire experiment (Figure 3). This is because a comparison of the GPP trajectory lines between the control run and the no-fire experiment (Figures 3a and 3b) suggested that wildfires depressed annual GPP by nearly the same extent throughout the 21st century and the no-fire/fixed-CO₂ experiment showed a decreasing GPP trend (Figure 3c). The no-fire/no-tree experiment also simulates a decreasing GPP trend during the 21st century (Figure 3d). The latter result can be explained by the fact that this experiment allowed plant establishment only for the C₄ grass PFT, which has a much lower CO₂ fertilization effect than other C₃ PFTs [Sato *et al.*, 2007].

For the continental-averaged GPP, the VPD formulation showed upward responses compared to its RH counterpart under a 21st century warming trend, while the continental-averaged transpiration rate showed the opposite trend, resulting in a higher increase in WUE for the VPD formulation than for the RH formulations.

This result may have been foreshadowed by the leaf-level equations. The basic equations for leaf-level CO₂ and water vapor fluxes across stomata are given by

$$p = \frac{gs}{1.6} (c_a - c_i) \tag{6}$$

$$tr = gs(e_i - e_a) \approx gs \text{ VPD}, \tag{7}$$

where p is the photosynthetic rate, tr is the transpiration rate, c_i is the intercellular CO₂ concentration, e_i is the intercellular vapor pressure, e_a is the atmospheric vapor pressure, and the coefficient 1.6 is the relative diffusivity of water vapor with respect to CO₂. In equation (7), the difference in vapor pressure between

Table 1. Results for Each of the Three Model Variants in the Control Experiment Averaged Over the Whole Continental Area^a

	Averages for 1991–2000			Changes Until 2091–2100 (%)		
	VPD Formulation	RH Modified Formulation	RH Original Formulation	VPD Formulation	RH Modified Formulation	RH Original Formulation
GPP (kg C m ⁻² yr ⁻¹)	0.69	0.68	0.69	15.6	15.0	14.7
NPP (kg C m ⁻² yr ⁻¹)	0.34	0.34	0.34	10.1	9.4	8.9
Runoff (mm yr ⁻¹)	243.4	236.4	238.9	24.1	23.6	23.1
Evapotranspiration (mm yr ⁻¹)	365.2	372.2	369.7	1.2	2.0	2.1
Foliage interception (mm yr ⁻¹)	63.0	63.0	63.2	2.4	3.0	2.7
Evaporation from bare ground (mm yr ⁻¹)	156.2	155.7	155.6	6.2	5.8	5.9
Transpiration (mm yr ⁻¹)	146.0	153.5	150.8	-4.7	-2.4	-1.9
WUE (g C m ⁻² mm ⁻¹)	33.2	30.3	31.3	26.9	22.0	21.2

^aTen-year averages at the end of the 20th century are presented along with their changes for the next 100 years. Bolded values show breakdown of the immediate upper row.

the inside and outside of stomata (i.e., $e_i - e_a$) is approximated by VPD because e_i is nearly saturated at a given air temperature and because boundary layer conductance is assumed to be much greater than stomatal conductance. Leaf-level WUE from equations (6) and (7) is defined as the ratio of p to tr and is given as

$$WUE = \frac{c_a \left(1 - \frac{c_i}{c_a}\right)}{1.6 \text{ VPD}} \quad (8)$$

By ignoring residual conductance (GS_{b1}) and the compensation point (Γ), both of which have much smaller values than other variables in equations (1) and (4), the fraction of intercellular and atmospheric CO₂ concentrations (c_i/c_a) can be approximated for each conductance formulation. Equations (1) and (6) for the VPD formulation yield

$$\frac{c_i}{c_a} \approx 1 - \frac{1.6}{GS_{b2}} \left(1 + \frac{\text{VPD}}{GS_{b3}}\right), \quad (9)$$

whereas equations (4) and (6) for the RH formulation yield

$$\frac{c_i}{c_a} \approx 1 - \frac{1.6}{GS_{b4 \text{ RH}}}. \quad (10)$$

Because RH is roughly invariant across climatic shifts between the present and the 21st century, as shown earlier, WUE does not markedly change. However, increasing VPD leads to a decrease in c_i/c_a , an increase in $1 - c_i/c_a$, and thus a higher WUE.

Higher WUE in the VPD formulation would explain its higher GPP. Increasing VPD and stable RH during the 21st century would result in relatively lower g_s for the VPD formulation than for the RH-modified formulation (refer to equations (1) and (4)). As lower g_s directly results in a lower photosynthesis rate p according to equation (6), it contradicts the intuitive understanding for the simulation results that the annual GPP at the end of the 21st century becomes higher for the VPD formulation than for the RH formulations. This would be explained by the negative feedback through the soil water content because higher g_s intensifies the transpiration rate, resulting in lower soil water content. For the area where vegetation productivity is distinctly limited by soil water content, WUE and not the immediate response of g_s would largely control the averaged GPP. A supportive evidence for the above discussion was obtained in the changes of the continental-averaged green day, which is defined as the days in a year with leaf area index more than 0.1 (m² m⁻²). At the end of the 20th century (averaged for the years during 1991 to 2000), the green day was 172.7, 172.1, and 172.7 (d yr⁻¹), respectively, for the VPD, RH-modified, and RH-original formulations. At the end of the 21st century (averaged for the years during 2091 to 2100), the green days are extended by 3.4, 2.2, and 2.1 (d yr⁻¹), respectively.

The eastern part of the African continent (areas within squared boxes in Figure 1) also shows higher GPP and WUE for the VPD formulation when referenced to the RH formulation under changing climate of the 21st century (Table 2). As VPD decreases during the 21st century in this region (Figure 1), the above explanation cannot be applied. This conserved response of the model can be explained by the

Table 2. Results for Each of the Three Model Variants in the Control Experiment Averaged Over Eastern Part of the Continent (Areas Within Squared Box in Figure 1)^a

	Averages for 1991–2000			Changes Until 2091–2100 (%)		
	VPD Formulation	RH Modified Formulation	RH Original Formulation	VPD Formulation	RH Modified Formulation	RH Original Formulation
GPP (kg C m ⁻² yr ⁻¹)	0.08	0.08	0.08	82.2	79.2	74.1
NPP (kg C m ⁻² yr ⁻¹)	0.04	0.04	0.04	75.8	72.9	67.2
Runoff (mm yr ⁻¹)	272.3	263.3	265.6	114.0	113.5	113.9
Evapotranspiration (mm yr ⁻¹)	577.5	586.5	584.2	21.5	23.2	22.6
Foliage interception (mm yr ⁻¹)	96.5	96.2	97.3	39.7	40.6	37.8
Evaporation from bare ground (mm yr ⁻¹)	259.2	258.5	256.2	-7.9	-8.7	-6.6
Transpiration (mm yr ⁻¹)	221.7	231.8	230.7	48.0	51.5	48.5
WUE (g C m ⁻² mm ⁻¹)	50.7	44.8	46.6	40.3	35.6	34.8

^aTen-year averages at the end of the 20th century are presented along with their changes for the next 100 years. Bolded values show breakdown of the immediate upper row.

counterbalance of concurrent increase of RH, which is only apparent for this region. Anyhow, this conserved response would demonstrate robustness of the different behavior of VPD and RH formulations under warming trends.

In contrast, the annual average GPP at the end of 21st century in the no-fire/no-tree experiment was lower for the VPD formulation than it was for the RH-modified formulation by about 0.033 (kg C m⁻² yr⁻¹) (Figure 3d). This experiment only allowed the establishment of the C₄ grass PFT, which has much higher WUE than other the PFTs [Sato *et al.*, 2007]. Accordingly, its annual transpiration (Appendix S6 in the supporting information) at the end of the 20th and 21st centuries was only about half those of the control and other runs (Table 1 and Appendices S4 and S5 in the supporting information), of which a large part of the GPP gains was by C₃ woody PFTs. Such a circumstance should relax the photosynthetic limitations imposed by soil water in the no-fire/no-tree experiment. Actually, changes in the geographical distribution of GPP during the 21st century (Appendix S2 in the supporting information) in this experiment were less correlated with changes in precipitation (Appendix S1 in the supporting information) compared to those for the control (and other) runs.

In all experiments, the RH formulations showed same trends of difference to the VPD formulation in the continental averages of GPP, the transpiration rate, and WUE until the end of the 21st century. Hence, our analysis would be valid irrespective of whether the CO₂ compensation point is included in the *g_s* function. In the no-fire/no-tree experiment, RH formulations showed nearly identical results in all simulated items (Figure 3d and Appendix S6 in the supporting information). This can be explained by the fact that the experiment only allowed the establishment of the C₄ grass PFT, whose CO₂ competition point is negligible (equation (3)). Hence, differences between the RH formulations are also minor.

Difference in GPP delivers cumulative effects in time on carbon pools in the form of biomass and soil organic carbon. In the control experiments, difference in carbon pools during the 21st century is larger for the VPD formulation than for the RH modified formulation by 4.9 (as biomass 3.8, as soil organic carbon 1.1) (PgC) and larger than for the RH original formulation by 3.3 (as biomass 2.6, as soil organic carbon 0.6) (PgC). These differences are comparable to the global anthropogenic carbon emission due to fossil fuel and cement production (5.5 ± 0.4 Pg C yr⁻¹), which is an annual estimate average over years 1980 to 1989 [Intergovernmental Panel on Climate Change, 2013].

4.1. Implication of the Findings

A wide variety of GCMs forecast a RH distribution that is largely insensitive to changes in climate [Held and Soden, 2000; Ingram, 2002; Manabe and Wetherald, 1975]. For example, in an analysis using an existing model archive of 21st century climate change experiments performed for the IPCC Fourth Assessment, it is shown that the water vapor feedback in GCMs is close to that which would result from a climate-invariant distribution of RH [Soden and Held, 2006]. This finding is also supported by long-term satellite measurements [Allan *et al.*, 2003]. This finding is now well supported by current GCMs [Ingram, 2002] and long-term satellite measurements [Allan *et al.*, 2003]. Despite large differences in forecasted changes in

VPD and minor changes in RH, and despite evidence that VPD is a more appropriate control for transpiration efficiency than RH [e.g., Aphalo and Jarvis, 1991; Nijs et al., 1997; Way et al., 2011], RH remains widely employed in ESMs and LSMs when stomatal conductance is computed (Appendix S3 in the supporting information). Our analysis suggests biases when employing the RH formulation for stomatal conductance under a current warming trend that can lead to underestimating the GPP and overestimating the transpiration rate, resulting in an underestimate of WUE. Note that for the carbon cycle, we mainly analyzed the difference in the annual GPP, but this difference leads to cumulative effects in time on carbon pools as biomass and soil organic carbon.

Acknowledgments

The data for this paper are available at author's website at http://seib-dgvm.com/hsato/data/SatoEtAl_StomataAfrica/. We thank the members of Department of Environmental Geochemical Cycle Research, Japan Agency for Marine-Earth Science and Technology for their fruitful discussions. This work was financially supported by the following grants: (a) the "Precise Impact Assessments on Climate Change" of the Program for Risk Information on Climate Change (SOUSEI Program) supported by the Ministry of Education, Culture, Sports, Science, and Technology-Japan (MEXT) and (b) MEXT/JSPS KAKENHI grant 25281003.

References

- Allan, R. P., M. A. Ringer, and A. Slingo (2003), Evaluation of moisture in the Hadley Centre climate model using simulations of HIRS water-vapour channel radiances, *Q. J. R. Meteorol. Soc.*, *129*(595), 3371–3389.
- Aphalo, P. J., and P. G. Jarvis (1991), Do stomata respond to relative-humidity, *Plant Cell Environ.*, *14*(1), 127–132.
- Ball, J. T., I. E. Woodrow, and J. A. Berry (1987), A model predicting stomatal conductance and its contribution to the control of photosynthesis under different environmental conditions, in *Progress in Photosynthesis Research*, edited by J. Biggens, pp. 221–224, Martinus Nijhoff Publishers, Dordrecht, Netherlands.
- Beer, C., et al. (2010), Terrestrial gross carbon dioxide uptake: Global distribution and covariation with climate, *Science*, *329*(5993), 834–838.
- Brooks, A., and G. D. Farquhar (1985), Effect of temperature on the CO₂/O₂ specificity of ribulose-1,5-bisphosphate carboxylase oxygenase and the rate of respiration in the light: Estimates from gas-exchange measurements on spinach, *Planta*, *165*(3), 397–406.
- Buckley, T. N. (2005), The control of stomata by water balance, *New Phytol.*, *168*(2), 275–291.
- Collatz, G. J., J. T. Ball, C. Grivet, and J. A. Berry (1991), Physiological and environmental-regulation of stomatal conductance, photosynthesis and transpiration: A model that includes a laminar boundary-layer, *Agric. For. Meteorol.*, *54*(2–4), 107–136.
- Collatz, G. J., M. Ribas-Carbo, and J. A. Berry (1992), Coupled photosynthesis-stomatal conductance model for leaves of C₄ plants, *Aust. J. Plant Physiol.*, *19*(5), 519–538.
- Damour, G., T. Simonneau, H. Cochard, and L. Urban (2010), An overview of models of stomatal conductance at the leaf level, *Plant Cell Environ.*, *33*(9), 1419–1438.
- Emori, S., A. Hasegawa, T. Suzuki, and K. Dairaku (2005), Validation, parameterization dependence, and future projection of daily precipitation simulated with a high-resolution atmospheric GCM, *Geophys. Res. Lett.*, *32*, L06708, doi:10.1029/2004GL022306.
- Held, I. M., and B. J. Soden (2000), Water vapor feedback and global warming, *Annu. Rev. Energy Environ.*, *25*, 441–475.
- Ingram, W. J. (2002), On the robustness of the water vapor feedback: GCM vertical resolution and formulation, *J. Clim.*, *15*(9), 917–921.
- Intergovernmental Panel on Climate Change (2013), *Climate Change 2013: The Physical Science Basis. Contribution of Working Group I to the Fifth Assessment Report of the Intergovernmental Panel on Climate Change*, edited by T. F. Stocker et al., 1535 pp., Cambridge Univ. Press, Cambridge, U. K., and New York.
- Ito, A., and T. Oikawa (2002), A simulation model of the carbon cycle in land ecosystems (Sim-CYCLE): A description based on dry-matter production theory and plot-scale validation, *Ecol. Model.*, *151*(2–3), 143–176.
- Jarvis, P. G. (1976), Interpretation of variations in leaf water potential and stomatal conductance found in canopies in field, *Philos. Trans. R. Soc. B*, *273*(927), 593–610.
- K-1-Model-Developers (2004), K-1 coupled model (MIROC) description, Univ. of Tokyo.
- Kalnay, E., et al. (1996), The NCEP/NCAR 40-year reanalysis project, *Bull. Am. Meteorol. Soc.*, *77*(3), 437–471.
- Katul, G. G., S. Palmroth, and R. Oren (2009), Leaf stomatal responses to vapour pressure deficit under current and CO₂-enriched atmosphere explained by the economics of gas exchange, *Plant Cell Environ.*, *32*(8), 968–979.
- Katul, G. G., S. Manzoni, S. Palmroth, and R. Oren (2010), A stomatal optimization theory to describe the effects of atmospheric CO₂ on leaf photosynthesis and transpiration, *Ann. Bot.*, *105*(3), 431–442.
- Kumagai, T., T. M. Saitoh, Y. Sato, T. Morooka, O. J. Manfroi, K. Kuraji, and M. Suzuki (2004), Transpiration, canopy conductance and the decoupling coefficient of a lowland mixed dipterocarp forest in Sarawak, Borneo: Dry spell effects, *J. Hydrol.*, *287*(1–4), 237–251.
- Lambers, H., F. S. Chapin, and T. L. Pons (1998), *Plant Physiological Ecology*, Springer, New York.
- Leuning, R. (1995), A critical-appraisal of a combined stomatal-photosynthesis model for C-3 plants, *Plant Cell Environ.*, *18*(4), 339–355.
- Manabe, S., and R. T. Wetherald (1975), The effects of doubling the CO₂ concentration on the climate of a general circulation model, *J. Atmos. Sci.*, *32*(1), 3–15.
- Medlyn, B. E., R. A. Duursma, D. Eamus, D. S. Ellsworth, I. C. Prentice, C. V. M. Barton, K. Y. Crous, P. de Angelis, M. Freeman, and L. Wingate (2011), Reconciling the optimal and empirical approaches to modelling stomatal conductance, *Global Change Biol.*, *17*(6), 2134–2144.
- Mitchell, T. D., and P. D. Jones (2005), An improved method of constructing a database of monthly climate observations and associated high-resolution grids, *Int. J. Climatol.*, *25*(6), 693–712.
- Nijs, I., R. Ferris, H. Blum, G. Hendrey, and I. Impens (1997), Stomatal regulation in a changing climate: A field study using Free Air Temperature Increase (FATI) and Free Air CO₂ Enrichment (FACE), *Plant Cell Environ.*, *20*(8), 1041–1050.
- Prentice, I. C., N. Dong, S. M. Gleason, V. Maire, and I. J. Wright (2014), Balancing the costs of carbon gain and water transport: Testing a new theoretical framework for plant functional ecology, *Ecol. Lett.*, *17*(1), 82–91.
- Sato, H., and T. Ise (2012), Effect of plant dynamic processes on African vegetation responses to climate change: Analysis using the spatially explicit individual-based dynamic global vegetation model (SEIB-DGVM), *J. Geophys. Res.*, *117*, G03017, doi:10.1029/2012JG002056.
- Sato, H., A. Itoh, and T. Kohyama (2007), SEIB-DGVM: A new dynamic global vegetation model using a spatially explicit individual-based approach, *Ecol. Model.*, *200*(3–4), 279–307.
- Sellers, P. J., D. A. Randall, G. J. Collatz, J. A. Berry, C. B. Field, D. A. Dazlich, C. Zhang, G. D. Collelo, and L. Bounoua (1996), A revised land surface parameterization (SiB2) for atmospheric GCMs. 1: Model formulation, *J. Clim.*, *9*(4), 676–705.
- Soden, B. J., and I. M. Held (2006), An assessment of climate feedbacks in coupled ocean-atmosphere models, *J. Clim.*, *19*(14), 3354–3360.
- Way, D. A., R. Oren, H.-S. Kim, and G. G. Katul (2011), How well do stomatal conductance models perform on closing plant carbon budgets? A test using seedlings grown under current and elevated air temperatures, *J. Geophys. Res.*, *116*, G04031, doi:10.1029/2011JG001808.